



Ru(II)–halide–carbonyl complexes of naphthylazoimidazoles: Synthesis, spectra, electrochemistry, catalytic activity and electronic structure

Shyamal Kumar Sarkar¹, Mahendra Sekhar Jana, Tapan Kumar Mondal, Chittaranjan Sinha*

Department of Chemistry, Inorganic Chemistry Section, Jadavpur University, Kolkata 700032, India

ARTICLE INFO

Article history:

Received 16 April 2012

Received in revised form

31 May 2012

Accepted 13 June 2012

Keywords:

Naphthylazoimidazole

Ruthenium–carbonyl–halide

X-ray structure

Catalytic oxidation

Electrochemistry

DFT calculation

ABSTRACT

[Ru(CO)₂Cl₂(α/β -NaiR)] (**1**, **2**) and [Ru(CO)₂I₂(α/β -NaiR)] (**3**, **4**) are synthesized by the reaction of [Ru(CO)₂Cl₂]_n or [Ru(CO)₄I₂] with α/β -NaiR (1-alkyl-2-(naphthyl- α/β -azo)imidazole (α -NaiR/ β -NaiR, where, R = Me, CH₂CH₃ and CH₂Ph)) and have been characterized by spectroscopic data. The geometry of the representative complexes [Ru(CO)₂Cl₂(β -NaiMe)] (**2a**) and [Ru(CO)₂I₂(β -NaiEt)] (**4b**) have been structurally confirmed by X-ray diffraction study. The redox property is examined by electrochemistry. Catalytic activity of these compounds is investigated to the oxidation of PhCH₂OH to PhCHO, 2-butanol (C₄H₉OH) to 2-butanone, 1-phenylethanol (PhC₂H₄OH) to acetophenone, cyclopentanol (C₅H₉OH) to cyclopentanone and cyclohexanol to cyclohexanone by N-methylmorpholine-N-oxide (NMO), H₂O₂ or Bu^tOOH in CH₂Cl₂ and NMO shows highest yield. The catalytic efficiency is again dependent on Ru–X (X = Cl or I) bond and higher yield is observed for [Ru(CO)₂Cl₂(α/β -NaiR)] (**1**, **2**). Electronic structure, spectral and redox properties are explained based on DFT and TD-DFT calculations on the representative complexes.

© 2012 Elsevier B.V. All rights reserved.

1. Introduction

The transition metal–polypyridine complexes are attracting much for their spectroscopic, electrochemical, photophysical, photochemical properties and their therapeutic and catalytic applications [1–7]. The structures, spectra and electrochemical properties of ruthenium complexes of azoimine function (–N=N–C=N–) and the correlation with calculated electronic structure and composition of MOs have been described extensively [8–12]. They have been used as catalysts and photo-catalysts for water oxidation [13] or oxidation of organic compounds [14,15]. The oxidation of alcohols plays an important role in organic synthesis and the efforts are continuing for the development of new oxidative processes [16–18]. The traditional methods for oxidation using stoichiometric amount of inorganic oxidants in high temperature and pressure cause serious environmental problems and have lower selectivity [19]. It would be of great economical and ecological importance to develop processes, which take place at milder conditions and causes less environmental pollution. With this view, in the past few decades there has been a growing interest in transition metal-catalyzed oxidation of alcohols

using oxidants such as air, molecular oxygen, hydrogen peroxide, *tert*-butyl hydroperoxide and N-methylmorpholine-N-oxide (NMO) [20–29]. Among the second row transition metal ions, ruthenium mediated oxidations are finding application because its oxidation state can vary from +II to +VIII [30–33].

We have been engaged in the last few years to develop ruthenium–carbonyl chemistry of diimine and azoimine functionalized heterocyclic ligands [34–38]. We report herein, the synthesis, crystal and electronic structures, spectroscopic properties of hitherto new ruthenium(II)–carbonyl complexes (**1–4**) of 1-alkyl-2-(naphthyl- α/β -azo)imidazoles (α -NaiR/ β -NaiR, where R = Me, CH₂CH₃ and CH₂Ph) (Scheme 1). The catalytic activity of the complexes for the oxidation of primary and secondary alcohols to the respective aldehyde and ketones are studied using N-methylmorpholine-N-oxide (NMO) and peroxides (H₂O₂, Bu^tOOH) as oxidizing agents.

2. Results and discussion

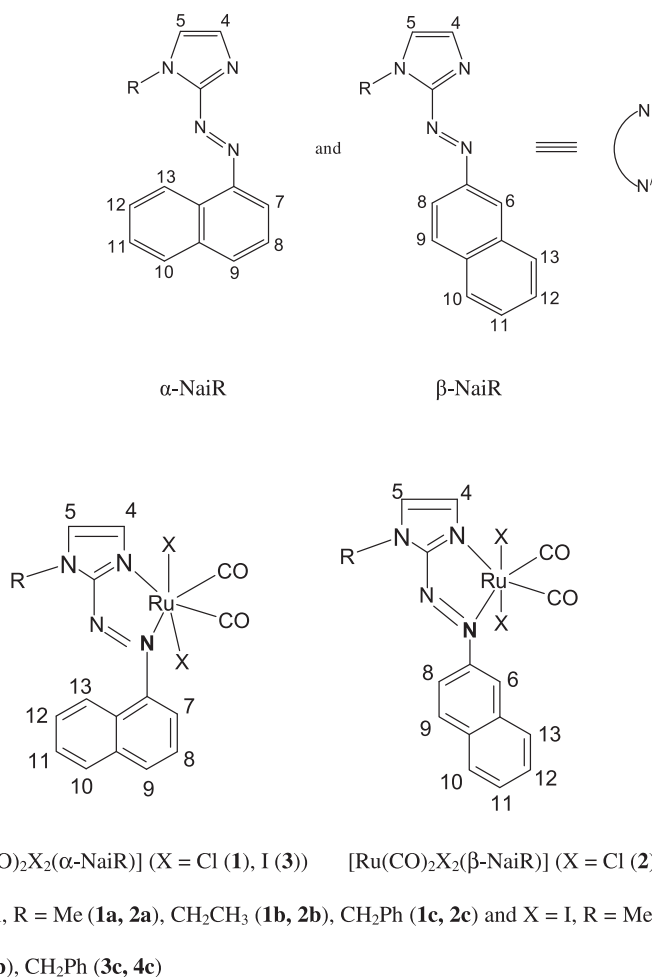
2.1. Synthesis and formulation

The reaction of 1-alkyl-2-(naphthyl- α/β -azo)imidazoles (α/β -NaiR, where R = CH₃, CH₂CH₃ and CH₂Ph) with [Ru(CO)₂Cl₂]_n in dry MeCN in inert (N₂) environment under refluxing condition for 6 h has resulted dark red solution and the complexes [Ru(CO)₂Cl₂(α/β -

* Corresponding author. Fax: +91 033 2413 7121.

E-mail address: c_r_sinha@yahoo.com (C. Sinha).

¹ Present address: Department of Chemistry, Uluberia College, Uluberia, Howrah 711315, India.



Scheme 1.

NaiR)] (**1**, **2**) are isolated by evaporation of the solvent (Scheme 1). The purification of the complexes has been carried out by chromatographic process. $[\text{Ru}(\text{CO})_2\text{I}_2(\alpha/\beta\text{-NaiR})]$ (**3**, **4**) have been synthesized by reacting $[\text{Ru}(\text{CO})_4\text{I}_2]$ with $\alpha/\beta\text{-NaiR}$ following the similar reaction conditions. All the complexes, **1–4** are diamagnetic and the microanalytical and spectral data support the composition. The structural confirmation in case of $[\text{Ru}(\text{CO})_2\text{Cl}_2(\beta\text{-NaiMe})]$ (**2a**) and $[\text{Ru}(\text{CO})_2\text{I}_2(\beta\text{-NaiEt})]$ (**4b**) have been established by single crystal X-ray diffraction studies.

2.2. Infrared and ¹H NMR spectra

The complexes show two equally intense $\nu(\text{CO})$ bands at 1995–2006 and 2048–2065 cm^{-1} which supports the *cis*- $\text{Ru}(\text{CO})_2$ configuration [36–38]. Infrared spectra of the complexes also exhibit $\nu(\text{C}=\text{N})$ at 1542–1563 cm^{-1} and $\nu(\text{N}=\text{N})$ at 1355–1365 cm^{-1} (see Experimental section). The azo ($-\text{N}=\text{N}-$) stretching is significantly shifted to lower frequency region compared to free ligand value (1400–1410 cm^{-1}), which supports $d\pi(\text{Ru}) \rightarrow \pi^*(\text{N}=\text{N})$ back donation in the complexes [39,40].

The ¹H NMR spectra of all the complexes are recorded in CDCl₃ solution. The ¹H NMR signals of the complexes are shifted to downfield side compare to free ligand value (see Experimental section) [39] which may be due to strong retrobonding effect of CO ($d\pi(\text{Ru}) \rightarrow \pi^*(\text{CO})$). Imidazole protons, 4- and 5-H appear as a broad singlet at 7.75–7.85 and 7.45–7.55 ppm, respectively and

have been downfield shifted ($\Delta\delta = 0.60\text{--}0.80$ ppm). The singlet nature of imidazole protons may be due to rapid proton exchange at the NMR time scale with solvent proton (may be coming from moisture during measurement). The 1-R signals of $\alpha/\beta\text{-NaiR}$ appear at their usual position [39,40]. 1-Me appears as a singlet at 4.25–4.30 ppm; 1-CH₂-CH₃ gives a quartet (4.51–4.67 ppm, $J = 8.0$ Hz) and a triplet (1.67–1.71 ppm ($J = 7.0$ Hz)) respectively; 1-CH₂-(Ph) gives a singlet at 5.69–5.85 ppm. The Ru–X bonds have significant control over proton signal position; in general $[\text{Ru}(\text{CO})_2\text{Cl}_2(\alpha\text{-NaiR})]$ (**1**) and $[\text{Ru}(\text{CO})_2\text{Cl}_2(\beta\text{-NaiR})]$ (**2**) show higher chemical shift than $[\text{Ru}(\text{CO})_2\text{I}_2(\alpha\text{-NaiR})]$ (**3**) and $[\text{Ru}(\text{CO})_2\text{I}_2(\beta\text{-NaiR})]$ (**4**).

2.3. Molecular structures

The molecular structures of $[\text{Ru}(\text{CO})_2\text{Cl}_2(\beta\text{-NaiMe})]$ (**2a**) and $[\text{Ru}(\text{CO})_2\text{I}_2(\beta\text{-NaiEt})]$ (**4b**) are shown in Figs. 1 and 2, respectively; selected bond parameters are listed in Table 1. The structure is similar to $[\text{Ru}(\text{CO})_2\text{Cl}_2(1\text{-ethyl-2-(phenylazo)imidazole})]$ [38]. Ru atom is in a distorted octahedral geometry with $\text{RuC}_2\text{X}_2(\text{N},\text{N}')$ coordination sphere (N, N' refer to N(imidazole) and N(azo) donor centers respectively of $\beta\text{-NaiMe}$ in **2a** and $\beta\text{-NaiEt}$ in **4b**) (X = Cl in **2a** and I in **4b**). The atomic arrangements in the coordination sphere involve two *trans*-X (Cl or I), a chelated 1-methyl or ethyl-2-(naphthyl- β -azo)imidazole ($\beta\text{-NaiMe}$ in **2a** and $\beta\text{-NaiEt}$ in **4b**) and two *cis*-CO within the coordination sphere. The *trans*-X,X angles,

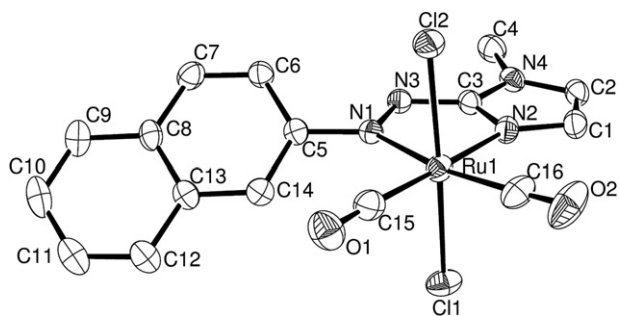


Fig. 1. ORTEP plot of $[\text{Ru}(\text{CO})_2\text{Cl}_2(\beta\text{-NaiMe})]$ (**2a**) (35% ellipsoidal probability).

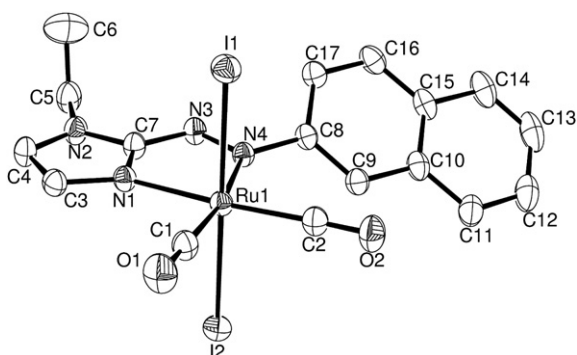


Fig. 2. ORTEP plot of $[\text{Ru}(\text{CO})_2\text{I}_2(\beta\text{-NaiEt})]$ (**4b**) (35% ellipsoidal probability).

$\text{X}(1)\text{--Ru--X}(2)$ are of $174.83(6)^\circ$ and $176.95(1)^\circ$ in **2a** and **4b** respectively. The deviation of the coordination sphere from the ideal octahedron is due to the small bite angle of the five membered chelate ring ($\text{Ru}(1)\text{--N}(1)\text{--N}(3)\text{--C}(3)\text{--N}(2)$, $74.85(18)^\circ$ in **2a** and $\text{Ru}(1)\text{--N}(1)\text{--C}(7)\text{--N}(3)\text{--N}(4)$, $75.37(11)^\circ$ in **4b**). Other angles

about Ru define the distorted octahedral geometry in the complexes.

The Ru–N(azo) distance ($\text{Ru}(1)\text{--N}(1)$, $2.145(4)$ Å in **2a**) and ($\text{Ru}(1)\text{--N}(4)$, $2.130(3)$ Å in **4b**) is significantly longer than Ru–N(imidazole) distance $\text{Ru}(1)\text{--N}(2)$, $2.072(5)$ Å in **2a** and ($\text{Ru}(1)\text{--N}(1)$, $2.093(3)$ Å in **4b**). In general the Ru–N(azo) bond distance is shorter than Ru–N(imidazole) bond length which may be due to better $d\pi(\text{Ru}) \rightarrow \pi^*(\text{N}=\text{N})$ back donation than imidazole–N. Because of stronger π -acidity of CO than $\text{--N}=\text{N}\text{--}$ function coordinated *trans* to each other may reduce $d\pi(\text{Ru}) \rightarrow \pi^*(\text{N}=\text{N})$ back donation process and may be responsible for elongation of Ru–N(azo) lengths compared to reported bond lengths [34]. The azo bond lengths in the complexes are $1.265(7)$ Å in **2a** and $1.278(4)$ Å in **4b** respectively and are closer to free ligand azo distance, $1.267(3)$ Å [41]. The azo distance for non-carbonyl ruthenium complexes with this ligand system was found to be longer than present complexes [39,42].

2.4. DFT calculation: electronic structure and spectra

The full geometry optimizations were carried out for the representative complexes **2a** and **4b** using DFT method. The calculated bond distances and angles are well reproduced the X-ray data (Table 1). Selected molecular orbitals along with energy and composition for **2a** and **4b** are summarized in Supplementary Tables S1 and S2 respectively. Contour plots of some selected molecular orbitals are given in Figs. 3 and 4 for **2a** and **4b** respectively. The higher energy occupied orbitals (HOMO and HOMO – 1) for **2a** have 32–37% ruthenium character along with 55–62% contribution from Cl. In **4b** the corresponding orbitals have less ruthenium contribution (15–19%) and increased iodide character (79–83%). The high energy occupied orbitals, HOMO – 2 to HOMO – 6 have mixed ligand and halide $p\pi$ character. In both **2a** and **4b** the LUMO has ligand character (90–93%) with a HOMO–LUMO energy gap 2.62 eV and 2.33 eV in **2a** and **4b**

Table 1
Bond distances (Å) and angles ($^\circ$) of $[\text{Ru}(\text{CO})_2\text{Cl}_2(\beta\text{-NaiMe})]$ (**2a**) and $[\text{Ru}(\text{CO})_2\text{I}_2(\beta\text{-NaiEt})]$ (**4b**).

Bond distances (Å)	2a		Bond distances (Å)	4b	
	X-ray	Calc.		X-ray	Calc.
Ru(1)–N(1)	2.145(4)	2.193	Ru(1)–N(1)	2.093(3)	2.093
Ru(1)–N(2)	2.072(5)	2.129	Ru(1)–N(4)	2.130(3)	2.129
Ru(1)–Cl(1)	2.3723(15)	2.454	Ru(1)–I(1)	2.6966(9)	2.696
Ru(1)–Cl(2)	2.3804(15)	2.457	Ru(1)–I(2)	2.7059(9)	2.705
Ru(1)–C(15)	1.135(10)	1.889	Ru(1)–C(1)	1.881(4)	1.884
Ru(1)–C(16)	1.090(9)	1.883	Ru(1)–C(2)	1.885(4)	1.881
C(15)–O(1)	1.135(10)	1.150	C(1)–O(1)	1.127(5)	1.131
C(16)–O(2)	1.090(9)	1.149	C(2)–O(2)	1.131(5)	1.127
N(1)–N(3)	1.265(7)	1.277	N(3)–N(4)	1.278(4)	1.278
Bond angles ($^\circ$)					
N(1)–Ru(1)–N(2)	74.85(18)	74.52	N(1)–Ru(1)–N(4)	75.37(11)	75.37
N(1)–Ru(1)–Cl(1)	88.82(11)	89.37	N(1)–Ru(1)–I(1)	88.48(9)	88.48
N(1)–Ru(1)–Cl(2)	86.06(11)	86.21	N(1)–Ru(1)–I(2)	90.22(9)	90.22
N(1)–Ru(1)–C(15)	101.4(2)	99.41	N(1)–Ru(1)–C(1)	95.88(15)	174.6
N(1)–Ru(1)–C(16)	169.1(2)	170.0	N(1)–Ru(1)–C(2)	174.63(15)	95.88
N(2)–Ru(1)–Cl(1)	88.27(12)	90.05	N(4)–Ru(1)–I(1)	85.53(7)	85.53
N(2)–Ru(1)–Cl(2)	89.67(12)	86.29	N(4)–Ru(1)–I(2)	91.47(7)	91.47
N(2)–Ru(1)–C(15)	176.1(2)	173.3	N(4)–Ru(1)–C(1)	171.08(14)	99.30
N(2)–Ru(1)–C(16)	94.6(2)	95.58	N(4)–Ru(1)–C(2)	99.30(15)	171.1
Cl(1)–Ru(1)–Cl(2)	174.83(6)	174.8	I(1)–Ru(1)–I(2)	176.95(1)	176.9
Cl(1)–Ru(1)–C(15)	90.65(17)	92.71	I(1)–Ru(1)–C(1)	92.57(12)	90.43
Cl(1)–Ru(1)–C(16)	93.56(17)	92.00	I(1)–Ru(1)–C(2)	90.43(12)	92.57
Cl(2)–Ru(1)–C(15)	91.09(17)	90.53	I(2)–Ru(1)–C(1)	90.31(12)	90.61
Cl(2)–Ru(1)–C(16)	91.33(17)	90.90	I(2)–Ru(1)–C(2)	90.61(12)	90.30
C(15)–Ru(1)–C(16)	89.3(3)	90.40	C(1)–Ru(1)–C(2)	89.42(18)	89.42
Ru(1)–C(15)–O(1)	177.5(5)	178.7	Ru(1)–C(1)–O(1)	177.9(3)	177.9
Ru(1)–C(16)–O(2)	177.0(6)	177.5	Ru(1)–C(2)–O(2)	178.0(4)	177.9

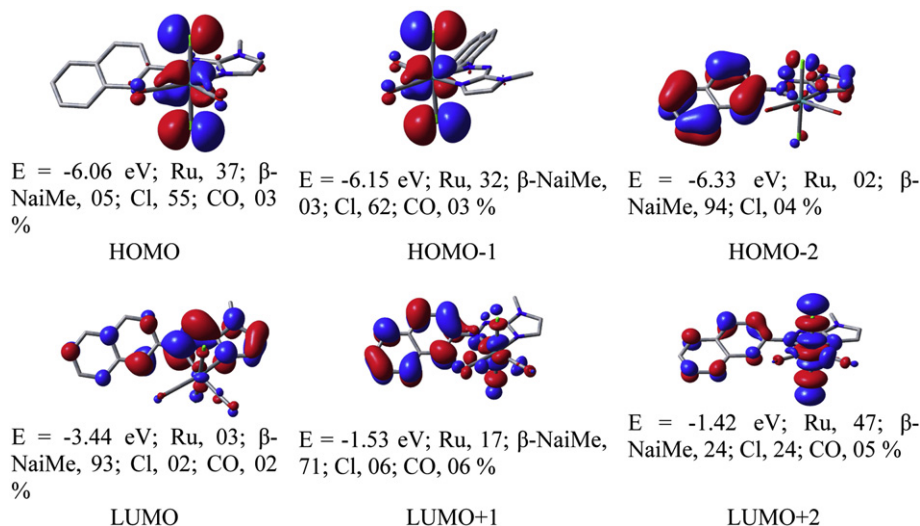


Fig. 3. Contour plots of some selected molecular orbitals of $[\text{Ru}(\text{CO})_2\text{Cl}_2(\beta\text{-NaiMe})]$ (**4a**).

respectively. LUMO + 3 to LUMO + 5 show high degree of mixing between $\text{Ru}(d\pi)$ and $\pi^*(\text{CO})$.

To further study the electronic structures of the complexes NBO calculations on the optimized geometry of **2a** and **4b** were performed. The polarity of the bonds is accounted on Natural bond orbital (NBO) analysis. The Ru–C has one natural bond orbital while each C–O has three natural bond orbitals. The Ru–C bond orbitals are usually polarized the carbon atom, and subsequently the C–O bond orbitals are polarized the oxygen. The occupancies and hybridization of the CO and Ru–C bonds are summarized in Supplementary Table S3. The NBO charge of Ru atom is 0.038 and 0.021 in **2a** and **4b**, respectively, which are much lower than +2 formal charge. The charge on carbon atom of carbonyl groups is +0.693 (C15), +0.708 (C16) in **2a** and +0.665 (C1), +0.642 (C2) in **4b**, oxygen atom is negative -0.434 (O1), -0.434 (O2) in **2a** and -0.421 (O1), -0.422 (O2) in **4b** (Supplementary Table S4). The highly populated antibonding NBOs (0.3021–0.3048 in **2a** and 0.3314–0.3416 in **4b**)

indicate the higher extent of back donation from $d\pi(\text{Ru}) \rightarrow \pi^*(\text{CO})$. This in fact influences stretching frequency of CO ($\nu(\text{CO})$ in the complexes) $1995\text{--}2006$ and $2048\text{--}2065$ $\text{cm}^{-1} < \nu(\text{CO})$ in free state), 2143 cm^{-1}).

The absorption spectra of the complexes are measured at room temperature in dry acetonitrile (Fig. 5), and the experimental absorption bands are assigned based on singlet–singlet vertical excitations calculated by TD-DFT/CPCM method in acetonitrile on the optimized geometry of **2a** and **4b**. Some of the calculated excitation wavelength and their assignment are given in Table 2 and Table 3 for **2a** and **4b**, respectively. The complexes **2a** and **4b** show moderately intense band at 473 nm and 485 nm respectively corresponds to HOMO – 1 \rightarrow LUMO, mixed MLCT and XLCT transitions. The band at 411 nm and 367 nm for **2a** and **4b** respectively has ILCT/XLCT character. In addition the intense bands at 390–310 nm for the complexes are purely intra-ligand charge transfer transitions (ILCT).

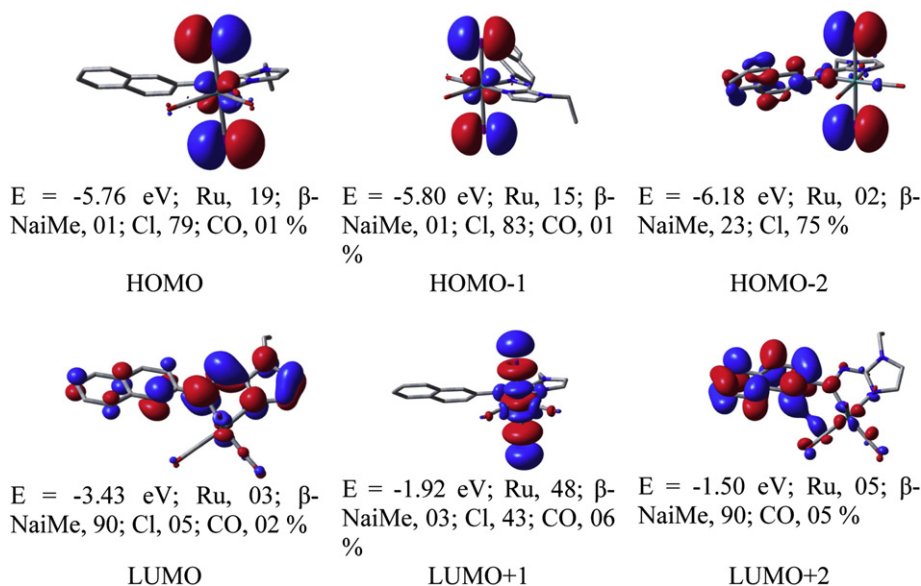


Fig. 4. Contour plots of some selected molecular orbitals of $[\text{Ru}(\text{CO})_2\text{I}_2(\beta\text{-NaiEt})]$ (**4b**).

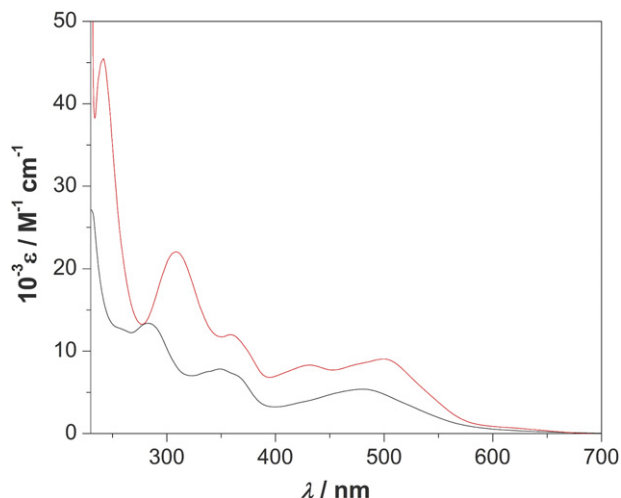


Fig. 5. UV-vis spectra of $[\text{Ru}(\text{CO})_2\text{Cl}_2(\alpha\text{-NaiMe})]$ (**1a**) (—) and $[\text{Ru}(\text{CO})_2\text{I}_2(\alpha\text{-NaiMe})]$ (**3a**) (—) in acetonitrile.

2.5. Electrochemistry

The complexes, **1** and **2**, show one quasi-reversible oxidation at 1.19–1.33 V (ΔE , 125–135 mV) and one reductive response, $-(0.44\text{--}0.55\text{ V})$ (ΔE , 77–86 mV) along with one irreversible, $-(1.13\text{--}1.27\text{ V})$ reduction. The compounds, **3** and **4** show one quasi-reversible, 1.39–1.48 V (ΔE , 115–125 mV) and one irreversible, 0.62–0.67 V oxidative response positive to reference Ag/AgCl electrode along with one reversible reductive responses, $-(0.53\text{--}0.57\text{ V})$ (ΔE , 80–87 mV) and one irreversible, $-(1.27\text{--}1.33\text{ V})$ reductive response (Fig. 6, Table 4).

The redox couples have been assigned on the basis of DFT results. The HOMO and HOMO – 1 of **4b** have 17–19% Ru character and 79–83% iodine contribution. So, the first irreversible oxidation in complexes **3** and **4** has been assigned as $\text{I}^-/\frac{1}{2}\text{I}_2$ oxidation and the quasi-reversible second oxidation at higher potential range is $\text{Ru}^{\text{II}}/\text{Ru}^{\text{III}}$ couple. Although Cl contributes 55% character to HOMO of **2a** but its energy is about 0.30 eV stabilized more than that of **4b** and thus $\text{Cl}^-/\frac{1}{2}\text{Cl}_2$ oxidation is not feasible. In **2a** the ruthenium contribution to HOMO and HOMO – 1 has been increased to 32–37% than that of **4b** and the oxidation has been assigned as $\text{Ru}^{\text{II}}/\text{Ru}^{\text{III}}$ couple in complexes **1**, **2**. LUMOs of the complexes exclusively have ligand character with 44–48% azo contribution, so the reductions are taking place on azo bond in all the complexes leading to the formation of $\text{L}^{\cdot-}$ on first and L^{2-} after second reductions respectively.

Table 2
Calculated singlet–singlet vertical electronic transitions for $[\text{Ru}(\text{CO})_2\text{Cl}_2(\beta\text{-NaiMe})]$ (**2a**) in acetonitrile.

Excitation (eV)	$\lambda_{\text{excitation}}$ (nm)	Osc. strength (f)	Key transition	Character
2.3336	531.3	0.0101	(72%)HOMO → LUMO	$\text{Ru}(d\pi)/\text{Cl}(p\pi) \rightarrow \beta\text{-NaiMe}(\pi^*)$ (MLCT, XLCT)
2.5447	487.2	0.0674	(84%)HOMO – 1 → LUMO	$\text{Ru}(d\pi)/\text{Cl}(p\pi) \rightarrow \beta\text{-NaiMe}(\pi^*)$ (MLCT, XLCT)
2.7758	446.7	0.1165	(72%)HOMO – 6 → LUMO	$\beta\text{-NaiMe}(\pi)/\text{Cl}(p\pi) \rightarrow \beta\text{-NaiMe}(\pi^*)$ (ILCT/XLCT)
3.5987	344.5	0.0753	(32%)HOMO – 7 → LUMO (20%)HOMO – 6 → LUMO	$\beta\text{-NaiMe}(\pi)/\text{Cl}(p\pi) \rightarrow \beta\text{-NaiMe}(\pi^*)$ (ILCT/XLCT)
4.1229	300.7	0.0353	(61%)HOMO – 10 → LUMO	$\beta\text{-NaiMe}(\pi) \rightarrow \beta\text{-NaiMe}(\pi^*)$ (ILCT)
4.2259	293.4	0.0411	(43%)HOMO – 2 → LUMO + 4 (23%)HOMO – 10 → LUMO	$\beta\text{-NaiMe}(\pi) \rightarrow \beta\text{-NaiMe}(\pi^*)$ (ILCT)
4.4620	277.9	0.1219	(59%)HOMO – 12 → LUMO	$\beta\text{-NaiMe}(\pi) \rightarrow \beta\text{-NaiMe}(\pi^*)$ (ILCT)

2.6. Catalytic oxidation

Catalytic oxidation of benzyl alcohol (PhCH_2OH), 2-butanol ($\text{C}_4\text{H}_9\text{OH}$), 1-phenylethanol ($\text{PhC}_2\text{H}_4\text{OH}$), cyclopentanol ($\text{C}_5\text{H}_9\text{OH}$) and cyclohexanol (CyCH-OH) was carried out using $[\text{Ru}(\text{CO})_2\text{X}_2(\alpha/\beta\text{-NaiR})]$ ($\text{X} = \text{Cl}$ or I and $\text{R} = \text{Me}$ or Et) as catalyst and *N*-methylmorpholine-*N*-oxide (NMO)/ H_2O_2 (30%)/ Bu^tOOH as oxidant in CH_2Cl_2 in refluxing condition for an appropriate period of time. The complexes catalyze the oxidation of PhCH_2OH to PhCHO , $\text{C}_4\text{H}_9\text{OH}$ to $\text{C}_4\text{H}_7\text{O}$ (2-butanone), $\text{PhC}_2\text{H}_4\text{OH}$ to PhCOCH_3 (acetophenone), $\text{C}_5\text{H}_9\text{OH}$ to $\text{C}_5\text{H}_8\text{O}$ (cyclopentanone) and CyCH-OH to CyC=O (cyclohexanone) with high yields and the results are given in Table 5, Supplementary Tables S5 and S6. The aldehyde or ketone formed after 1 h of reflux was determined by GC and there was no detectable oxidation in the absence of ruthenium complex. Results of the investigations suggest that the complexes are able to react efficiently with NMO or peroxides ($\text{H}_2\text{O}_2/\text{Bu}^t\text{OOH}$) to yield a high valent ruthenium-oxo species [43,44], which is capable of oxygen atom transfer to alcohols. The residue has been dried by evaporation. The volatile organic matter may be evaporated during drying of oxidation product; however, the existence of $\text{Ru}(\text{IV})=\text{O}$ species ($[\text{Ru}(\alpha/\beta\text{-NaiR}) = \text{O}]^*$) has been proved by FT-IR spectra [44,45] ($\sim 860\text{ cm}^{-1}$). The catalyst is also susceptible to generate oxidation products like CO_2 and $\text{XO}_3^-/\text{XO}_4^-$. We do not have any technical support to collect CO_2 and its measurement but presence of halate (ClO_3^- and IO_3^-) is identified qualitatively by manganous sulfate-phosphoric acid test [46]. A plausible oxidation loop is given in Fig. 7. The oxidation activity follows $\text{NMO} > \text{Bu}^t\text{OOH} > \text{H}_2\text{O}_2$ which may be due to their inbuilt oxygen transfer efficiency to the catalyst. The catalytic efficiency of $[\text{Ru}(\text{CO})_2\text{Cl}_2(\alpha/\beta\text{-NaiR})]$ (**1**, **2**) is higher than $[\text{Ru}(\text{CO})_2\text{I}_2(\alpha/\beta\text{-NaiR})]$ (**3**, **4**) which may be due to the consumption of oxidant for some unidentified reaction (oxidation of iodide!). Besides, $\text{Ru}(\alpha\text{-NaiR})$ -compounds (**1**, **3**) show better catalytic activity than $\text{Ru}(\beta\text{-NaiR})$ -compounds (**2**, **4**). Out of these five alcohols cyclohexanol and 1-phenylethanol show higher product conversion ratio than others and least activity is observed for 2-butanol. The compounds reported in this article show comparable catalytic efficiency with reported catalysts for supporting oxidation of alcohols by NMO or peroxides such as Ru-azophelato compounds [47] or Ru-Schiff bases [48].

3. Experimental section

3.1. Materials and instrumentation

The 1-alkyl-2-(naphthyl- α/β -azo)imidazoles were synthesized following a previously published procedure [39]. $[\text{Ru}(\text{CO})_2\text{Cl}_2]_n$ and

Table 3
Calculated singlet–singlet vertical electronic transitions for $[\text{Ru}(\text{CO})_2\text{I}_2(\beta\text{-NaiEt})]$ (**4b**) in acetonitrile.

$E_{\text{excitation}}$ (eV)	$\lambda_{\text{excitation}}$ (nm)	Osc. strength (f)	Key transition	Character
2.2587	548.9	0.0075	(96%)HOMO \rightarrow LUMO	$\text{Ru}(d\pi)/\text{I}(\text{p}\pi) \rightarrow \beta\text{-NaiEt}(\pi^*)$ (MLCT, XLCT)
2.5012	495.7	0.1035	(77%)HOMO – 1 \rightarrow LUMO	$\text{Ru}(d\pi)/\text{I}(\text{p}\pi) \rightarrow \beta\text{-NaiEt}(\pi^*)$ (MLCT, XLCT)
3.0094	412.0	0.1723	(77%)HOMO – 5 \rightarrow LUMO	$\beta\text{-NaiEt}(\pi)/\text{I}(\text{p}\pi) \rightarrow \beta\text{-NaiEt}(\pi^*)$ (ILCT, XLCT)
3.2345	383.3	0.1268	(83%)HOMO – 6 \rightarrow LUMO	$\beta\text{-NaiEt}(\pi)/\text{I}(\text{p}\pi) \rightarrow \beta\text{-NaiEt}(\pi^*)$ (ILCT, XLCT)
3.9896	310.8	0.0793	(65%)HOMO – 11 \rightarrow LUMO	$\beta\text{-NaiEt}(\pi) \rightarrow \beta\text{-NaiEt}(\pi^*)$ (ILCT)
4.2394	292.4	0.0485	(69%)HOMO – 2 \rightarrow LUMO + 2	$\beta\text{-NaiEt}(\pi)/\text{I}(\text{p}\pi) \rightarrow \beta\text{-NaiEt}(\pi^*)$ (ILCT, XLCT)
4.4070	281.3	0.0714	(67%)HOMO – 12 \rightarrow LUMO + 2	$\beta\text{-NaiEt}(\pi) \rightarrow \beta\text{-NaiEt}(\pi^*)$ (ILCT)
4.5786	270.8	0.1396	(39%)HOMO – 4 \rightarrow LUMO + 2 (30%)HOMO – 2 \rightarrow LUMO + 4	$\beta\text{-NaiEt}(\pi)/\text{I}(\text{p}\pi) \rightarrow \beta\text{-NaiEt}(\pi^*)$ (ILCT, XLCT)

$[\text{Ru}(\text{CO})_4\text{I}_2]$ were prepared by a reported method [36,49]. Imidazole and all other organic chemicals and inorganic salts were available from Sisco Research Lab, Mumbai, India. All other chemicals and solvents were of reagent grade and were used without further purification. Commercially available SRL silica gel (60–120 mesh) was used for column chromatography.

Microanalytical data (C, H, N) were collected on Perkin–Elmer 2400 CHNS/O elemental analyzer. Infrared spectra were taken on a RX-1 Perkin Elmer spectrophotometer with samples prepared as KBr pellets. UV–vis spectral studies were performed on a Perkin Elmer Lambda 25 spectrophotometer. ^1H NMR spectra were recorded using a Bruker (AC) 300 MHz FTNMR spectrometer in CDCl_3 . Cyclic voltammetric measurements were carried out using a CH1 Electrochemical workstation. A platinum wire working electrode, a platinum wire auxiliary electrode and Ag/AgCl reference electrode were used in a standard three-electrode configuration. $[\text{Bu}_4\text{N}][\text{ClO}_4]$ was used as the supporting electrolyte and the scan rate used was 50 mV s^{-1} in dry acetonitrile under N_2 atmosphere. The reported potentials are uncorrected for junction potential. The catalytic yields were determined using Agilent 7890 series Gas chromatography instrument equipped with a flame ionization detector (FID) using a HP-5 column of 30 m length, 0.53 mm diameter and 5.00 μm film thickness.

3.2. Synthesis of complexes

3.2.1. Synthesis of $[\text{Ru}(\text{CO})_2\text{Cl}_2(\alpha\text{-NaiMe})]$ (**1a**)

To a 20 mL acetonitrile suspension of $[\text{Ru}(\text{CO})_2\text{Cl}_2]_n$ (100 mg, 0.43 mmol) 15 mL acetonitrile solution of $\alpha\text{-NaiMe}$ (**1a**) (103.63 mg,

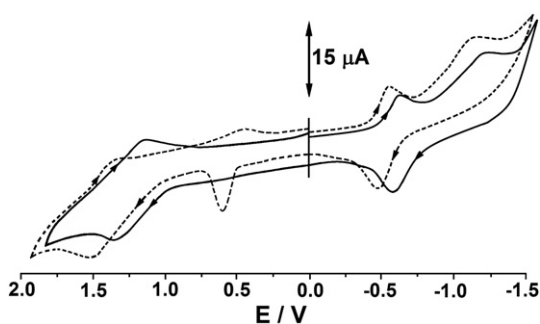


Fig. 6. Cyclic voltammogram of $[\text{Ru}(\text{CO})_2\text{Cl}_2(\alpha\text{-NaiMe})]$ (**1a**) (—) and $[\text{Ru}(\text{CO})_2\text{I}_2(\beta\text{-NaiEt})]$ (**4b**) (---) in acetonitrile solution, supporting electrolyte Bu_4NClO_4 (0.1 M), reference electrode Ag/AgCl at scan rate of 50 mV s^{-1} .

0.44 mmol) was added and the reaction mixture was refluxed for 6 h under N_2 atmosphere. The color of the solution changed from orange to dark red. The solvent was removed under reduced pressure. The dark red dry mass was then dissolved in minimum volume of CH_2Cl_2 and subjected to chromatography separation on a silica gel column (60–120 mesh). The desired red band of **1a** was eluted by 1:10 CH_2Cl_2 –MeCN mixture. Slow evaporation of the solvent the red crystalline complex **1a** was obtained. The yield was 141.92 mg (72%). The other compounds **1b**, **1c**, **2a**, **2b** and **2c** were synthesized following the same procedure by the reaction of $[\text{Ru}(\text{CO})_2\text{Cl}_2]_n$ with $\alpha/\beta\text{-NaiR}$ ligands in the same molar ratio (1:1). The yields were about (65–74)%.

Microanalytical data: Calc. (found). For $\text{C}_{16}\text{H}_{12}\text{N}_4\text{OCl}_2\text{Ru}$ (**1a**): C, 41.40 (41.28); H, 2.61 (2.64); N, 12.07 (12.03). IR data (KBr disc) (cm^{-1}): 2005, 2065 $\nu(\text{CO})$, 1563 $\nu(\text{C}=\text{N})$, 1362 $\nu(\text{N}=\text{N})$. ^1H NMR data in CDCl_3 (ppm): 7.82 (4-H, s), 7.47 (5-H, s), 4.28 (N– CH_3 , s), 8.75 (7-H, d, $J = 7.60 \text{ Hz}$), 8.34 (13-H, d, $J = 9.74 \text{ Hz}$), 7.63 (8,9-H, m), 8.05 (10,13-H, m). UV–vis (CH_3CN): λ_{max} (ϵ , $\text{M}^{-1} \text{ cm}^{-1}$): 482 (13,481), 350 (19,834), 283 (33,532). For $\text{C}_{17}\text{H}_{14}\text{N}_4\text{OCl}_2\text{Ru}$ (**1b**): C, 42.69 (42.79); H, 2.95 (2.90); N, 10.04 (10.07). IR data (KBr disc) (cm^{-1}): 2006, 2062 $\nu(\text{CO})$, 1548 $\nu(\text{C}=\text{N})$, 1365 $\nu(\text{N}=\text{N})$. ^1H NMR data in CDCl_3 (ppm): 7.80 (4-H, s), 7.51 (5-H, s), 4.51 (N– CH_2 – CH_3 , q, $J = 7.50 \text{ Hz}$), 1.67 (N– CH_2 – CH_3 , t, $J = 7.00 \text{ Hz}$), 8.74 (7-H, d, $J = 7.50 \text{ Hz}$), 8.31 (13-H, d, $J = 8.75 \text{ Hz}$), 7.60 (8,9-H, m), 8.09 (10,13-H, m). UV–vis (CH_3CN): λ_{max} (ϵ , $\text{M}^{-1} \text{ cm}^{-1}$): 470 (12,350),

Table 4
Cyclic voltammetric data^a of **1–4**.

Complexes	E ($1^{-}/1/2$) ^b (V)	$E_{1/2}$ ($\text{Ru}^{\text{II}}/\text{Ru}^{\text{III}}$) (V) (ΔE_p , mV)	$E_{1/2}$ (L/L^{-}) ^d (V) (ΔE_p , mV)	E (L^{-}/L^2) ^{c,d} (V)
1a		1.27(127)	–0.44(77)	–1.13
1b		1.20(133)	–0.50(83)	–1.21
1c		1.19(125)	–0.47(82)	–1.16
2a		1.33(130)	–0.55(85)	–1.22
2b		1.25(135)	–0.53(77)	–1.27
2c		1.23(133)	–0.52(86)	–1.21
3a	0.63	1.47(115)	–0.55(85)	–1.27
3b	0.65	1.48(120)	–0.53(87)	–1.29
3c	0.62	1.43(117)	–0.54(80)	–1.30
4a	0.65	1.39(122)	–0.53(85)	–1.30
4b	0.67	1.42(125)	–0.57(80)	–1.33
4c	0.62	1.43(120)	–0.56(87)	–1.27

^a In acetonitrile solution, supporting electrolyte Bu_4NClO_4 (0.1 M), reference electrode Ag/AgCl , scan rate = 50 mV s^{-1} . $E_{1/2} = 0.5 (E_{\text{pa}} + E_{\text{pc}})$ where E_{pa} and E_{pc} are anodic and cathodic peak potentials, respectively; $\Delta E_p = E_{\text{pa}} - E_{\text{pc}}$.

^b Anodic potential.

^c Cathodic potential.

^d L = Chelated $\alpha/\beta\text{-NaiR}$.

Table 5
Catalytic oxidation of alcohols by Ru(II) complexes (**1–4**) using NMO as co-oxidant.

Complex	Substrate	Product	Yield ^a (%)	Turnover ^b (%)
1a	Benzyl alcohol	Benzaldehyde	78	78
	2-Butanol	2-Butanone	76	76
	1-Phenylethanol	Acetophenone	84	84
	Cyclopentanol	Cyclopentanone	82	82
1b	Cyclohexanol	Cyclohexanone	84	84
	Benzyl alcohol	Benzaldehyde	85	85
	2-Butanol	2-Butanone	79	79
	1-Phenylethanol	Acetophenone	89	89
1c	Cyclopentanol	Cyclopentanone	86	86
	Cyclohexanol	Cyclohexanone	90	90
	Benzyl alcohol	Benzaldehyde	79	79
	2-Butanol	2-Butanone	75	75
2a	1-Phenylethanol	Acetophenone	84	84
	Cyclopentanol	Cyclopentanone	80	80
	Cyclohexanol	Cyclohexanone	83	83
	Benzyl alcohol	Benzaldehyde	74	74
2b	2-Butanol	2-Butanone	71	71
	1-Phenylethanol	Acetophenone	77	77
	Cyclopentanol	Cyclopentanone	75	75
	Cyclohexanol	Cyclohexanone	78	78
2c	Benzyl alcohol	Benzaldehyde	86	86
	2-Butanol	2-Butanone	79	79
	1-Phenylethanol	Acetophenone	90	90
	Cyclopentanol	Cyclopentanone	86	86
3a	Cyclohexanol	Cyclohexanone	90	90
	Cyclohexanol	Cyclohexanone	90	90
	Benzyl alcohol	Benzaldehyde	77	77
	2-Butanol	2-Butanone	75	75
3b	1-Phenylethanol	Acetophenone	80	80
	Cyclopentanol	Cyclopentanone	79	79
	Cyclohexanol	Cyclohexanone	81	81
	Benzyl alcohol	Benzaldehyde	66	66
3c	2-Butanol	2-Butanone	64	64
	1-Phenylethanol	Acetophenone	68	68
	Cyclopentanol	Cyclopentanone	67	67
	Cyclohexanol	Cyclohexanone	70	70
4a	Benzyl alcohol	Benzaldehyde	72	72
	2-Butanol	2-Butanone	66	66
	1-Phenylethanol	Acetophenone	78	78
	Cyclopentanol	Cyclopentanone	74	74
4b	Cyclohexanol	Cyclohexanone	78	78
	Benzyl alcohol	Benzaldehyde	64	64
	2-Butanol	2-Butanone	62	62
	1-Phenylethanol	Acetophenone	72	72
4c	Cyclopentanol	Cyclopentanone	67	67
	Cyclohexanol	Cyclohexanone	73	73
	Benzyl alcohol	Benzaldehyde	70	70
	2-Butanol	2-Butanone	67	67
4a	1-Phenylethanol	Acetophenone	74	74
	Cyclopentanol	Cyclopentanone	71	71
	Cyclohexanol	Cyclohexanone	74	74
	Benzyl alcohol	Benzaldehyde	73	73
4b	2-Butanol	2-Butanone	69	69
	1-Phenylethanol	Acetophenone	81	81
	Cyclopentanol	Cyclopentanone	77	77
	Cyclohexanol	Cyclohexanone	80	80
4c	Benzyl alcohol	Benzaldehyde	71	71
	2-Butanol	2-Butanone	67	67
	1-Phenylethanol	Acetophenone	73	73
	Cyclopentanol	Cyclopentanone	72	72
Cyclohexanol	Cyclohexanone	73	73	

Substrate (1 mmol); NMO (3 mmol); complex (0.01 mmol); solvent dichloromethane.

^a Yield of product was determined using Agilent 7890 series Gas chromatography instrument equipped with a flame ionization detector (FID) using a HP-5 column of 30 m length, 0.53 mm diameter and 5.00 μm film thickness.

^b Moles of product per mole of catalyst.

360 (17,742), 275 (35,423). For $C_{22}H_{17}N_4O_2Cl_2Ru$ (**1c**): C, 48.90 (48.83); H, 2.98 (2.94); N, 10.37 (10.34). IR data (KBr disc) (cm^{-1}): 2005, 2059 $\nu(CO)$, 1549 $\nu(C=N)$, 1363 $\nu(N=N)$. ¹H NMR data in $CDCl_3$ (ppm): 7.85 (4-H, s), 7.53 (5-H, s), 5.85 (N-CH₂-Ph, s), 8.77 (7-H, d, $J = 7.62$ Hz), 8.33 (13-H, d, $J = 8.72$ Hz), 7.65 (8,9-H, m),

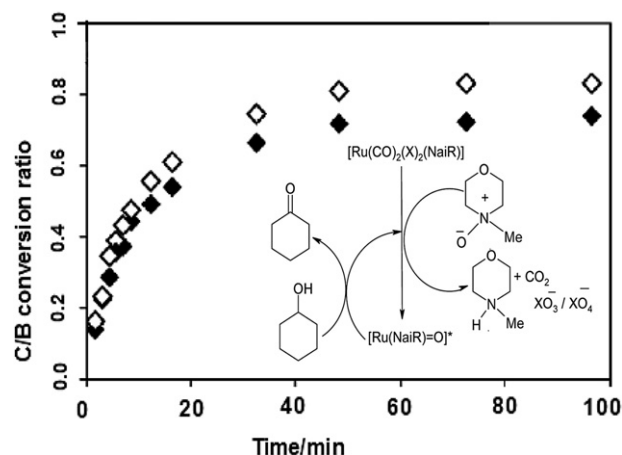


Fig. 7. Cyclohexanol (C, □) and benzyl alcohol (B, ■) oxidation product conversion ratio in presence of $[Ru(CO)_2Cl_2(\alpha-NaiMe)]$ (**3a**) in CH_2Cl_2 under reflux and plausible catalytic loop.

8.10 (10,13-H, m). UV-vis (CH_3CN): λ_{max} (ϵ , $M^{-1} cm^{-1}$): 487 (10,117), 355 (15,822), 282 (39,350). For $C_{16}H_{12}N_4O_2Cl_2Ru$ (**2a**): C, 41.39 (41.37); H, 2.61 (2.56); N, 12.07 (12.00). IR data (KBr disc) (cm^{-1}): 2000, 2053 $\nu(CO)$, 1546 $\nu(C=N)$, 1357 $\nu(N=N)$. ¹H NMR data in $CDCl_3$ (ppm): 7.83 (4-H, s), 7.45 (5-H, s), 4.29 (N-CH₃, s), 8.76 (6-H, s), 8.13 (8-H, d, $J = 6.64$ Hz), 8.12 (9-H, d, $J = 7.38$ Hz), 7.66 (10,13-H, m), 7.96 (11,12-H, m). UV-vis (CH_3CN): λ_{max} (ϵ , $M^{-1} cm^{-1}$): 473 (7854), 367 (11,532), 289 (31,453). For $C_{17}H_{14}N_4O_2Cl_2Ru$ (**2b**): C, 42.69 (42.74); H, 2.95 (2.90); N, 10.04 (10.09). IR data (KBr disc) (cm^{-1}): 1998, 2052 $\nu(CO)$, 1551 $\nu(C=N)$, 1361 $\nu(N=N)$. ¹H NMR data in $CDCl_3$ (ppm): 7.78 (4-H, s), 7.55 (5-H, s), 8.73 (6-H, s), 4.57 (N-CH₂-CH₃, q, $J = 7.60$ Hz), 1.70 (N-CH₂-CH₃, t, $J = 7.00$), 8.17 (8-H, d, $J = 6.60$ Hz), 8.15 (9-H, d, $J = 7.50$ Hz), 7.63 (10,13-H, m), 7.97 (11,12-H, m). UV-vis (CH_3CN): λ_{max} (ϵ , $M^{-1} cm^{-1}$): 465 (6915), 371 (10,781), 291 (35,626). For $C_{22}H_{17}N_4O_2Cl_2Ru$ (**2c**): C, 48.90 (48.93); H, 2.98 (2.93); N, 10.37 (10.30). IR data (KBr disc) (cm^{-1}): 1996, 2055 $\nu(CO)$, 1556 $\nu(C=N)$, 1360 $\nu(N=N)$. ¹H NMR data in $CDCl_3$ (ppm): 7.75 (4-H, s), 7.50 (5-H, s), 5.77 (N-CH₂-Ph, s), 8.15 (8-H, d, $J = 6.65$ Hz), 8.15 (9-H, d, $J = 9.80$ Hz), 7.68 (10,13-H, m), 7.95 (11,12-H, m). UV-vis (CH_3CN): λ_{max} (ϵ , $M^{-1} cm^{-1}$): 483 (5637), 361 (9852), 285 (29571).

3.2.2. Synthesis of $[Ru(CO)_2I_2(\alpha-NaiMe)]$ (**3a**)

The complex **3a** was prepared by the reaction of $[Ru(CO)_4I_2]$ (100 mg, 0.21 mmol) with α -NaiMe (**1a**) (51.82 mg, 0.22 mmol) following the same procedure as of **1a**. The purification was carried out by column chromatography. Yield was 73.79 mg (69%). Compounds **3b**, **3c**, **4a**, **4b** and **4c** were prepared following the same procedure by the reaction of $Ru(CO)_4I_2$ with α/β -NaiR ligands in the same molar ratio (1:1). The yields were about (67–72)%.

Microanalytical data: Calc. (found) For $C_{16}H_{12}N_4O_2I_2Ru$ (**3a**): C, 29.69 (29.59); H, 1.87 (1.83); N, 8.66 (8.60). IR data (KBr disc) (cm^{-1}): 1996, 2049 $\nu(CO)$, 1543 $\nu(C=N)$, 1360 $\nu(N=N)$. ¹H NMR data in $CDCl_3$ (ppm): 7.85 (4-H, s), 7.49 (5-H, s), 4.25 (N-CH₃, s), 8.61 (7-H, d, $J = 7.56$ Hz), 8.23 (13-H, d, $J = 9.76$ Hz), 7.66 (8,9-H, m), 7.89 (10,13-H, m). UV-vis (CH_3CN): λ_{max} (ϵ , $M^{-1} cm^{-1}$): 499 (8092), 431 (7440), 359 (10,734), 309 (19,945). For $C_{17}H_{14}N_4O_2I_2Ru$ (**3b**): C, 30.88 (30.81); H, 2.13 (2.10); N, 8.47 (8.53). IR data (KBr disc) (cm^{-1}): 2004, 2051 $\nu(CO)$, 1547 $\nu(C=N)$, 1358 $\nu(N=N)$. ¹H NMR data in $CDCl_3$ (ppm): 7.51 (4-H, s), 7.52 (5-H, s), 4.60 (N-CH₂-CH₃, q, $J = 7.70$ Hz), 1.67 (N-CH₂-CH₃, t, $J = 7.20$ Hz), 8.63 (7-H, d, $J = 8.00$ Hz), 8.29 (13-H, d, $J = 8.90$ Hz), 7.64 (8,9-H, m), 7.90 (10,13-H, m). UV-vis (CH_3CN): λ_{max} (ϵ , $M^{-1} cm^{-1}$): 497 (6091), 430 (5954), 308 (14,592), 359 (8225). For $C_{22}H_{17}N_4O_2I_2Ru$ (**3c**): C, 36.54 (36.47);

H, 2.23 (2.27); N, 7.75 (7.67). IR data (KBr disc) (cm^{-1}): 2001, 2061 $\nu(\text{CO})$, 1544 $\nu(\text{C}=\text{N})$, 1353 $\nu(\text{N}=\text{N})$. ^1H NMR data in CDCl_3 (ppm): 7.85 (4-H, s), 7.46 (5-H, s), 5.69 (N- CH_2 -Ph, s), 8.67 (7-H, d, $J = 7.49$ Hz), 8.13 (13-H, d, $J = 8.09$ Hz), 7.54 (8,9-H, m), 7.66 (10,13-H, m). UV-vis (CH_3CN): λ_{max} (ϵ , $\text{M}^{-1} \text{cm}^{-1}$): 504 (6774), 437 (5771), 308 (15,904), 361 (8282). For $\text{C}_{16}\text{H}_{12}\text{N}_4\text{O}_2\text{I}_2\text{Ru}$ (**4a**): C, 29.70 (29.74); H, 1.87 (1.83); N, 8.66 (8.71). IR data (KBr disc) (cm^{-1}): 2001, 2064 $\nu(\text{CO})$, 1542 $\nu(\text{C}=\text{N})$, 1358 $\nu(\text{N}=\text{N})$. ^1H NMR data in CDCl_3 (ppm): 7.80 (4-H, s), 7.45 (5-H, s), 8.69 (6-H, s), 4.30 (N- CH_3 , s), 8.10 (8-H, d, $J = 6.70$ Hz), 8.18 (9-H, d, $J = 8.73$ Hz), 7.96 (10,13-H, m), 7.65 (11,12-H, m). UV-vis (CH_3CN): λ_{max} (ϵ , $\text{M}^{-1} \text{cm}^{-1}$): 486 (6781), 410 (11,793), 312 (10,914). For $\text{C}_{17}\text{H}_{14}\text{N}_4\text{O}_2\text{I}_2\text{Ru}$ (**4b**): C, 30.88 (30.84); H, 2.13 (2.10); N, 8.47 (8.42). IR data (KBr disc) (cm^{-1}): 2000, 2053 $\nu(\text{CO})$, 1561 $\nu(\text{C}=\text{N})$, 1360 $\nu(\text{N}=\text{N})$. ^1H NMR data in CDCl_3 (ppm): 7.81 (4-H, s), 7.48 (5-H, s), 8.70 (6-H, s), 4.67 (N- CH_2 - CH_3 , q, $J = 7.32$ Hz), 1.71 (N- CH_2 - CH_3 , t, $J = 7.31$ Hz), 8.09 (8-H, d, $J = 6.58$ Hz), 8.15 (9-H, d, $J = 8.22$ Hz), 7.64 (10,13-H, m), 7.96 (11,12-H, m). UV-vis (CH_3CN): λ_{max} (ϵ , $\text{M}^{-1} \text{cm}^{-1}$): 485 (9112), 411 (15,545), 309 (12,864). For $\text{C}_{22}\text{H}_{17}\text{N}_4\text{O}_2\text{I}_2\text{Ru}$ (**4c**): C, 36.54 (36.49); H, 2.23 (2.27); N, 7.75 (7.78). IR data (KBr disc) (cm^{-1}): 2002, 2056 $\nu(\text{CO})$, 1563 $\nu(\text{C}=\text{N})$, 1359 $\nu(\text{N}=\text{N})$. ^1H NMR data in CDCl_3 (ppm): 7.79 (4-H, s), 7.46 (5-H, s), 8.69 (6-H, s), 5.77 (N- CH_2 -Ph, s), 8.09 (8-H, d, $J = 6.75$ Hz), 8.17 (9-H, d, $J = 8.96$ Hz), 7.64 (10,13-H, m), 7.96 (11,12-H, m). UV-vis (CH_3CN): λ_{max} (ϵ , $\text{M}^{-1} \text{cm}^{-1}$): 491 (8315), 411 (15,164), 312 (14,219).

3.3. X-ray crystal structure analysis

Details of crystal analyses, data collection and structure refinement data are given in Table 6. Crystal mounting was done on glass fibers with epoxy cement. Single crystal data collections were performed with an automated Bruker SMART APEX CCD diffractometer. Unit cell parameters were determined from least-squares refinement of setting angles with θ in the range $2.70 \leq \theta \leq 26.00^\circ$ (**2a**) and $2.50 \leq \theta \leq 25.00^\circ$ (**4b**). Out of 13,064 collected data 3558 for **2a** and 19,238 collected data 3670 for **4b** with $I > 2\sigma(I)$ were used for structure solution. The hkl ranges are $-18 \leq h \leq 14$, $-10 \leq k \leq 11$, $-17 \leq l \leq 17$ for **2a** and $-19 \leq h \leq 19$, $-10 \leq k \leq 10$, $-17 \leq l \leq 17$ for **4b**. Reflection data were recorded using the ω scan technique. The structures were solved and refined by full-matrix least-squares techniques on

Table 6
Crystal data and details of the structure determination of **2a** and **4b**.

Compound	[Ru(CO) ₂ Cl ₂ (β -NaiMe)] (2a)	[Ru(CO) ₂ I ₂ (β -NaiEt)] (4b)
Formula	C ₁₆ H ₁₂ N ₄ O ₂ Cl ₂ Ru	C ₁₇ H ₁₄ N ₄ O ₂ I ₂ Ru
M_r	464.27	661.19
Crystal system	Monoclinic	Monoclinic
Space group	$P 2_1/c$	$P 2_1/c$
a [Å]	14.904(3)	16.612(5)
b [Å]	9.1824(17)	8.551(2)
c [Å]	13.988(3)	14.723(4)
β [°]	109.475(3)	94.321(4)
Cell volume [Å ³]	1804.8(6)	2085.5(10)
Z	4	4
μ [mm ⁻¹]	1.182	3.730
T [K]	293	298
ρ_{calcd} [g cm ⁻³]	1.709	2.106
Data/restraints/parameters	3558/0/226	3670/0/236
$R1^a$, $wR2^b$ [$I > 2\sigma(I)$]	0.0523, 0.0962	0.0280, 0.0706
$R1$, $wR2$ (all data)	0.1007, 0.1117	0.0302, 0.0721
GO ^c	1.00	1.10

^a $R = \sum |F_o - F_c| / \sum F_o$.

^b $wR = [\sum w(F_o^2 - F_c^2)^2 / \sum w(F_o^4)]^{1/2}$ are general but w are different, $w = 1/[\sigma^2(F^2) + (0.0556P)^2 + 2.1396P]$ for (**2a**); $w = 1/[\sigma^2(F^2) + (0.1085P)^2 + 0.6247P]$ for (**4b**) where $P = (F_o^2 + 2F_c^2)/3$.

F^2 using the SHELX-97 program [50,51]. The absorption corrections were done by the multi-scan technique. All data were corrected for Lorentz and polarization effects, and the non-hydrogen atoms were refined anisotropically. Hydrogen atoms were included in the refinement process as per the riding model. All non-hydrogen atoms were refined anisotropically. Hydrogen atoms were constrained to ride on the respective carbon atoms with isotropic displacement parameters equal to 1.2 times the equivalent isotropic displacement of their parent carbon atoms in all cases.

3.4. Procedure for catalytic oxidation of alcohols

Catalytic oxidation of primary alcohol to corresponding aldehyde and secondary alcohol to ketone by ruthenium(II) complexes were studied in the presence of NMO, H₂O₂ or Bu^tOOH as co-oxidant. A typical reaction using the complex as a catalyst and primary or secondary alcohol, as substrate at 1:100 molar ratio was described as follows. A solution of [Ru(CO)₂Cl₂(α -NaiEt)] (**1b**) (0.01 mmol) in CH₂Cl₂ (20 ml) was added to the mixture containing PhCH₂OH (1 mmol), NMO (3 mmol) and molecular sieves. The reaction mixture was refluxed for 1 h, and the solvent was then evaporated under reduced pressure. The residue was then extracted with diethyl ether (20 ml), concentrated to ≈ 1 ml and was analyzed by GC. The oxidation products were identified by GC co-injection with authentic samples. All other alcohols were oxidized following identical reaction protocol.

3.5. Computational methods

All computations were performed using the Gaussian03 (G03) [52] software. The Becke's three-parameter hybrid exchange functional and the Lee-Yang-Parr nonlocal correlation functional [53–55] (B3LYP) was used throughout. The 6-31G(d) basis set for C, H, N and O atoms, while MIDI! basis functions for Cl and I atoms were used [56]. LanL2TZ(f) basis set with effective core potential was employed for Ru atom [57]. The vibrational frequency calculations were performed to ensure that the optimized geometries represent the local minima and there are only positive Eigen values. Natural bond orbital analyses were performed using the NBO 3.1 module of Gaussian03 [58]. Vertical electronic excitations based on B3LYP optimized geometries were computed for the time-dependent density functional theory (TD-DFT) formalism [59–61] in acetonitrile using conductor-like polarizable continuum model (CPCM) [62–64]. Gauss Sum [65] was used to calculate the fractional contributions of various groups to each molecular orbital.

4. Conclusion

Ruthenium/Osmium(II)–CO complexes of azoimine functions from 1-alkyl-2-(naphthyl- α/β -azo)imidazoles (α/β -NaiR) are structurally and spectroscopically characterized. The redox properties of the compounds are studied by cyclic voltammetry experiment. The catalytic activity of the complexes has been examined to the oxidation of benzyl alcohol to aldehyde and cyclohexanol to cyclohexanone by NMO, H₂O₂ or Bu^tOOH as oxidant. Thus scope of catalytic reaction has unveiled new defining area and we are studying the oxidation and reduction reactions using platinum metals complexes of arylazoimidazoles.

Acknowledgments

Financial support from the Department of Science & Technology and University Grants Commission, New Delhi is gratefully acknowledged.

Appendix A. Supplementary material

Crystallographic data for the structures **2a** and **4b** have been deposited with the Cambridge Crystallographic Data center, CCDC No. 855664 (**2a**) and 855665 (**4b**) respectively. Copies of this information may be obtained free of charge from the Director, CCDC, 12 Union Road, Cambridge CB2 1EZ, UK (e-mail: deposit@ccdc.cam.ac.uk or [www:http://www.ccdc.cam.ac.uk](http://www.ccdc.cam.ac.uk)).

References

- [1] K. Kalyansundaram, M. Grätzel, *Coord. Chem. Rev.* 177 (1998) 347–414.
- [2] J. Reedijk, in: G. Wilkinson, J.A. McClerverty (Eds.), *Comprehensive Coordination Chemistry*, Pergamon, Oxford, UK, 1987.
- [3] K. Kalyansundaram, *Coord. Chem. Rev.* 46 (1982) 159–244.
- [4] J. Andersson, F. Puntoriero, S. Serroni, A. Yartsev, T. Pascher, T. Polivka, S. Campagna, V. Sundström, *Faraday Discuss.* 127 (2004) 295–305.
- [5] T.J. Meyer, *Pure Appl. Chem.* 58 (1986) 1193–1206.
- [6] A. Juris, V. Balzani, F. Barigelletti, S. Campagna, P. Belser, A. von Zelewsky, *Coord. Chem. Rev.* 84 (1988) 85–277.
- [7] V. Balzani, A. Juris, M. Venturi, S. Campagna, S. Serroni, *Chem. Rev.* 96 (1996) 759–834.
- [8] T. Kojima, T. Morimoto, T. Sakamoto, S. Miyazaki, S. Fukuzumi, *Chem. Eur. J.* 14 (2008) 8904–8915.
- [9] A.A. Vlcek, E.S. Dodsworth, W.J. Pietro, A.B.P. Lever, *Inorg. Chem.* 34 (1995) 1906–1913.
- [10] S. Serroni, S. Campagna, F. Puntoriero, C.D. Pietro, N.D. McClenaghan, F. Loisean, *Chem. Soc. Rev.* 30 (2001) 367–375.
- [11] B.K. Ghosh, A. Chakravorty, *Coord. Chem. Rev.* 95 (1989) 239–294.
- [12] M. Menon, A. Pramanik, A. Chakravorty, *Inorg. Chem.* 34 (1995) 3310–3316.
- [13] J.K. Hurst, *Coord. Chem. Rev.* 249 (2005) 313–328.
- [14] J.A. Treadway, J.A. Moss, T.J. Meyer, *Inorg. Chem.* 38 (1999) 4386–4387.
- [15] W. Chen, F.N. Rein, R.C. Rocha, *Angew. Chem. Int. Ed.* 48 (2009) 9672–9675.
- [16] R.H. Crabtree, A. Habib, 1,1-Oxidation by Chemical Methods, in: B.M. Trost, I. Fleming (Eds.), *Comprehensive Organic Synthesis*, Pergamon, Oxford, 1991, pp. 1–20.
- [17] M. Hudlick, *Oxidation in Organic Chemistry*, in: ACS Monographs, vol. 186, American Chemical Society, Washington DC, 1990.
- [18] R.A. Sheldon, J.K. Kochi, *Metal Catalyzed Oxidations of Organic Compounds*, Academic Press, New York, 1981.
- [19] P.T. Anastas, J.C. Warner, *Green Chemistry: Theory and Practice*, Oxford University Press, 2000.
- [20] T. Iwasawa, M. Tokunaga, Y. Obora, Y. Tsuji, *J. Am. Chem. Soc.* 126 (2004) 6554–6555.
- [21] Y. Uozumi, R. Nakao, H. Rhee, *J. Organomet. Chem.* 692 (2007) 420–427.
- [22] K. Mori, T. Hara, T. Mizugaki, K. Ebitani, K. Kaneda, *J. Am. Chem. Soc.* 126 (2004) 10657–10666.
- [23] B. Karimi, A. Zamani, J.H. Clark, *Organometallics* 24 (2005) 4695–4698.
- [24] H.-K. Kwong, P.-K. Lo, K.-C. Lau, T.-C. Lau, *Chem. Commun.* 47 (2011) 4273–4275.
- [25] H.R. Mardani, H. Golchoubian, *Tetrahedron Lett.* 47 (2006) 2349–2352.
- [26] G. Rothenberg, L. Feldberg, H. Wiener, Y. Sasson, *J. Chem. Soc. Perkin Trans. 2* (1998) 2429–2434.
- [27] G. Ferguson, A.N. Ajjou, *Tetrahedron Lett.* 44 (2003) 9139–9142.
- [28] A. Behr, K. Eusterwienmann, *J. Organomet. Chem.* 403 (1991) 215–219.
- [29] P. Singh, A.K. Singh, *Organometallics* 29 (2010) 6433–6442.
- [30] M. Pagliaro, S. Campestrini, R. Ciriminna, *Chem. Soc. Rev.* 34 (2005) 837–845.
- [31] R.A. Sheldon, I.W.C.E. Arends, G.-J.T. Brink, A. Dijkstra, *Acc. Chem. Res.* 35 (2002) 774–781.
- [32] K. Yamaguchi, N. Mizuno, *Angew. Chem. Int. Ed.* 41 (2002) 4538–4542.
- [33] T. Naota, H. Takaya, S.-I. Murahashi, *Chem. Rev.* 98 (1998) 2599–2660.
- [34] T. Mathur, J. Dinda, P. Datta, G. Mostafa, T.-H. Lu, C. Sinha, *Polyhedron* 25 (2006) 2503–2512.
- [35] T.K. Mondal, J. Dinda, J. Cheng, T.-H. Lu, C. Sinha, *Inorg. Chim. Acta* 361 (2008) 2431–2438.
- [36] P. Datta, S.K. Sarkar, T.K. Mondal, A.K. Patra, C. Sinha, *J. Organomet. Chem.* 694 (2009) 4124–4133.
- [37] T.K. Mondal, P. Raghavaiah, A.K. Patra, C. Sinha, *Inorg. Chem. Commun.* 13 (2010) 273–277.
- [38] T.K. Mondal, S.K. Sarker, P. Raghavaiah, C. Sinha, *Polyhedron* 27 (2008) 3020–3028.
- [39] P. Byabartta, P.K. Santra, T.K. Misra, C. Sinha, C.H.L. Kennard, *Polyhedron* 20 (2001) 905–913.
- [40] J. Dinda, K. Bag, C. Sinha, G. Mostafa, T.-H. Lu, *Polyhedron* 22 (2003) 1367–1376.
- [41] M. Shivakumar, K. Pramanik, P. Ghosh, A. Chakravorty, *Chem. Commun.* (1998) 2103–2104.
- [42] J. Dinda, S. Senapati, T. Mondal, A.D. Jana, M.Y. Chiang, T.-H. Lu, C. Sinha, *Polyhedron* 25 (2006) 1125–1132.
- [43] H. Masuda, T. Taga, K. Osaki, H. Sugimoto, *J. Am. Chem. Soc.* 103 (1981) 2199–2203.
- [44] M.M.T. Khan, C. Sreelatha, S.A. Mirza, G. Ramachandriaiah, S.H.R. Abdi, *Inorg. Chim. Acta* 154 (1988) 103–108.
- [45] A.M. El-Hendawy, A.H. Alkubaisi, A.E. Kourashy, M.M. Shanab, *Polyhedron* 12 (1993) 2343–2350.
- [46] A.I. Vogel, *A Text Book of Macro and Semimicro Qualitative Inorganic Analysis*, fourth ed. Logmans, 1962.
- [47] K. Naresh Kumar, R. Ramesh, Yu Liu, *J. Mol. Catal. A: Chem.* 265 (2007) 218–226.
- [48] V.V. Raju I, K.P. Balasubramanian I, C. Jayabalakrishnan II, V. Chinnusamy, *Nat. Sci.* 3 (2011) 542–550.
- [49] M.I. Bruce, G. Wilkinson, F.G.A. Stone, E.W. Abel (Eds.), *Ruthenium Carbonyls and Related Compounds*, *Comprehensive Organometallic Chemistry*, vol. 4, Pergamon Press, Oxford, 1982, pp. 661–690.
- [50] G.M. Sheldrick, SHELXS-97. Program for the Solution of Crystal Structure, University of Göttingen, 1997.
- [51] G.M. Sheldrick, SHELXL-97. Program for Crystal Structure Refinement, University of Göttingen, Germany, 1997.
- [52] M.J. Frisch, G.W. Trucks, H.B. Schlegel, G.E. Scuseria, M.A. Robb, J.R. Cheeseman, J.A. Montgomery Jr., T. Vreven, K.N. Kudin, J.C. Burant, J.M. Millam, S.S. Iyengar, J. Tomasi, V. Barone, B. Mennucci, M. Cossi, G. Scalmani, N. Rega, G.A. Petersson, H. Nakatsuji, M. Hada, M. Ehara, K. Toyota, R. Fukuda, J. Hasegawa, M. Ishida, T. Nakajima, Y. Honda, O. Kitao, H. Nakai, M. Klene, X. Li, J.E. Knox, H.P. Hratchian, J.B. Cross, V. Bakken, C. Adamo, J. Jaramillo, R. Gomperts, R.E. Stratmann, O. Yazyev, A.J. Austin, R. Cammi, C. Pomelli, J.W. Ochterski, P.Y. Ayala, K. Morokuma, G.A. Voth, P. Salvador, J.J. Dannenberg, V.G. Zakrzewski, S. Dapprich, A.D. Daniels, M.C. Strain, O. Farkas, D.K. Malick, A.D. Rabuck, K. Raghavachari, J.B. Foresman, J.V. Ortiz, Q. Cui, A.G. Baboul, S. Clifford, J. Cioslowski, B.B. Stefanov, G. Liu, A. Liashenko, P. Piskorz, I. Komaromi, R.L. Martin, D.J. Fox, T. Keith, M.A. Al-Laham, C.Y. Peng, A. Nanayakkara, M. Challacombe, P.M.W. Gill, B. Johnson, W. Chen, M.W. Wong, C. Gonzalez, J.A. Pople, Gaussian 03, Revision D.01, Gaussian, Inc., Wallingford CT, 2004.
- [53] A.D. Becke, *J. Chem. Phys.* 98 (1993) 5648–5652.
- [54] P.J. Stevens, J.F. Devlin, C.F. Chabalowski, M.J. Frisch, *J. Phys. Chem.* 98 (1994) 11623–11627.
- [55] C. Lee, W. Yang, R.G. Parr, *Phys. Rev. B* 37 (1988) 785–789.
- [56] R.E. Easton, D.J. Giesen, A. Welch, C.J. Cramer, D.G. Truhlar, *Theor. Chim. Acta* 93 (1996) 281–301.
- [57] A.W. Ehlers, M. Bohme, S. Dapprich, A. Gobbi, A. Hollwarth, V. Jonas, K.F. Kohler, R. Stegmann, A. Veldkamp, G. Frenking, *Chem. Phys. Lett.* 208 (1993) 111–114.
- [58] E.D. Glendening, A.E. Reed, J.E. Carpenter, F. Weinhold, NBO, Version 3.1.
- [59] R. Bauernschmitt, R. Ahlrichs, *Chem. Phys. Lett.* 256 (1996) 454–464.
- [60] R.E. Stratmann, G.E. Scuseria, M.J. Frisch, *J. Chem. Phys.* 109 (1998) 8218–8224.
- [61] M.E. Casida, C. Jamorski, K.C. Casida, D.R. Salahub, *J. Chem. Phys.* 108 (1998) 4439–4449.
- [62] V. Barone, M. Cossi, *J. Phys. Chem. A* 102 (1998) 1995–2001.
- [63] M. Cossi, V. Barone, *J. Chem. Phys.* 115 (2001) 4708–4717.
- [64] M. Cossi, N. Rega, G. Scalmani, V. Barone, *J. Comput. Chem.* 24 (2003) 669–796.
- [65] N.M. O'Boyle, A.L. Tenderholt, K.M. Langner, *J. Comput. Chem.* 29 (2008) 839–845.